Wavefront distortion of the reflected and diffracted beams produced by the thermoelastic deformation of a diffraction grating heated by a Gaussian laser beam

Patrick P. Lu, Amber L. Bullington, Peter Beyersdorf,* Stefan Traeger,† and Justin Mansell‡

Ginzton Laboratory, Stanford University, Stanford, California 94305-4085, USA

Ray Beausoleil

HP Laboratories, 13837 175th Place NE, Redmond, Washington 98052-2180, USA

Eric K. Gustafson, Robert L. Byer, and Martin M. Fejer**

Ginzton Laboratory, Stanford University, Stanford, California 94305-4085, USA

Received April 20, 2006; revised September 13, 2006; accepted September 18, 2006; posted September 26, 2006 (Doc. ID 70078); published February 14, 2007

It may be advantageous in advanced gravitational-wave detectors to replace conventional beam splitters and Fabry–Perot input mirrors with diffractive elements. In each of these applications, the wavefront distortions produced by the absorption and subsequent heating of the grating can limit the maximum useful optical power. We present data on the wavefront distortions induced in a laser probe beam for both the reflected and diffracted beams from a grating that is heated by a Gaussian laser beam and compare these results to a simple theory of the wavefront distortions induced by thermoelastic deformations. © 2007 Optical Society of America

OCIS codes: 000.2780, 050.1950, 120.3180, 120.6810.

1. INTRODUCTION

Many optical systems contain transmissive components such as lenses and beam splitters. Laser power incident on these is partially absorbed by their substrates. At high powers, substrate absorption produces wavefront distortions through thermal-lensing and thermoelastic distortions. This is especially relevant for advanced gravitational-wave interferometers,[1–4] which will require several kilowatts of circulating power at the beam splitter to obtain the required phase sensitivity. Both the generation and the handling of such high optical power will be challenging. Kilowatt-class laser designs for gravitational-wave interferometry based on Nd:YAG have been proposed,[5] and it is likely that lasers for this application will be a reality within the current decade. However, high laser power will produce wavefront distortions in both the beam splitters and Fabry–Perot input mirrors; these distortions are more likely to limit the circulating power in advanced gravitational-wave detectors than the available laser power. While advanced gravitational-wave interferometers will probably use some form of active thermal compensation to reduce the effects of laser beam heating-induced distortion,[6] it could be advantageous to eliminate the degradation caused by substrate absorption by using reflective rather than transmissive components.[7–12] The use of reflective optics not only eliminates substrate absorption and thermal lensing, it also allows for the use of substrate materials that are not optically transparent, thus increasing the list of possible materials available for this application.

In this paper, we present a model for the thermoelastic wavefront distortions caused by surface heating of reflective optics and compare it with experimental results for both the reflected and diffracted beams from a thermally loaded grating. We also make calculations comparing thermoelastic deformations of a surface-heated grating with thermal lensing due to substrate absorption in a transmissive beam splitter.

2. HELLO AND VINET'S ANALYSIS OF THERMOELASTIC DISTORTIONS

Thermoelastic distortions arise from nonuniform heating caused by light absorbed in the reflective and antireflective coatings on the surface of a mirror and in the mirror substrate. These problems were examined by Winkler *et al.* in 1991[13,14] using a simple thermal model of this effect based on dimensional analysis in gravitational-wave interferometers and produced estimates of the size of the effect agreeing to a factor of ~2 with the exact results previously obtained by Hello and Vinet[15,16] and discussed below.

Hello and Vinet[15,16] developed an exact result for the distortions induced in the surface of a right circular cylinder of radius a and thickness h, under thermal loading by surface absorption of a Gaussian light beam of $1/e^2$ ra-

dius w, including both conductive and radiative cooling. In the steady state, the difference of the temperature field inside the mirror and the surrounding temperature field, $T=T_{\mathrm{int}}-T_{\mathrm{ext}}$, obeys the Laplace equation,

$$\nabla^2 T(r,z)=0, \tag{1}$$

subject to the boundary conditions on the barrel ($r=a$), at the front surface (the plane $z=-h/2$), and at the back surface (the plane $z=h/2$):

$$-\kappa\frac{\partial T(a,z)}{\partial z}=4\sigma' T_{\mathrm{ext}}^3 T(a,z), -\kappa\frac{\partial T(r,-h/2)}{\partial z}$$

$$=\epsilon\frac{2P}{\pi w^2}\exp(-2r^2/w^2)-4\sigma' T_{\mathrm{ext}}^3 T(r,-h/2),$$

$$-\kappa\frac{\partial T(r,h/2)}{\partial z}=4\sigma' T_{\mathrm{ext}}^3 T(r,h/2). \tag{2}$$

These dictate the balance between the power absorbed from a Gaussian beam of power P and spot size w with an intensity profile,

$$I(r)=\frac{2P}{\pi w^2}\exp(-2r^2/w^2), \tag{3}$$

and the power radiated according to the Stefan–Boltzmann relation linearized in T, where ϵ is the fraction of the incident power absorbed, σ' is the Stefan–Boltzmann constant corrected for the emissivity of the material, and κ is the thermal conductivity of the mirror substrate. The coordinate system, geometry of the mirror, and the orientation of the Gaussian heating beam are shown in Fig. 1. In the analysis of Hello and Vinet, an exact solution for the temperature field is expressed as a Dini series, and then this temperature field is used to compute the thermoelastic surface distortions.

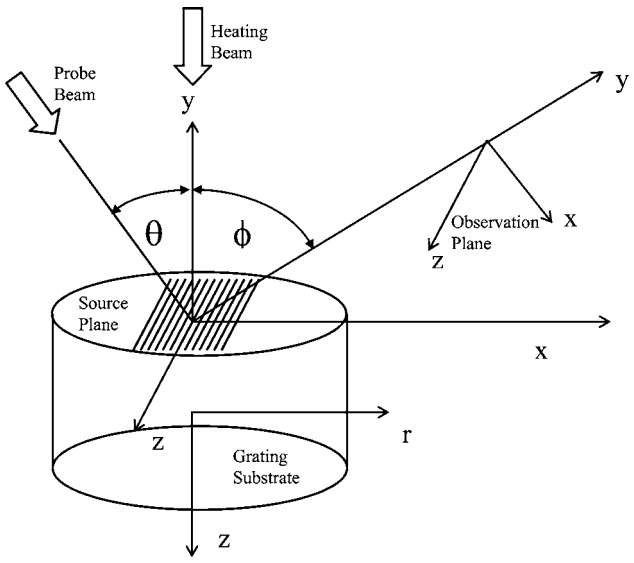

Fig. 1. Coordinate system and geometry used to calculate the temperature field and the thermoelastic distortions. Note that we have selected the same coordinate system as Hello and Vinet (Ref. 16) in which the heated surface is in the plane $z=-h/2$. The heating beam is normally incident on the grating.

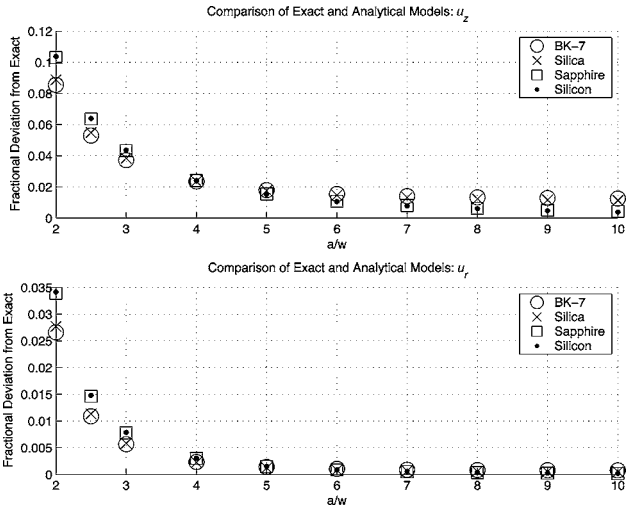

Fig. 2. Fractional deviation between the simplified theory and the exact model of Hello and Vinet versus optic size. The x axis indicates the scaling of the optic relative to a fixed beam size of $w=3.5$ cm. The aspect ratio of the optic was held fixed, with $h=a$. Fractional deviations were calculated at $r=2w$ by taking the difference between the simplified and exact theories and dividing by the exact theory. An emissivity of 0.5 was used.

3. SIMPLIFIED ANALYSIS

Here, we develop a simplified analysis, which reproduces the results of Hello and Vinet for most cases of interest and is convenient for design calculations. The approximate computation is based on the observation that cylindrical mirrors of radius $a>2w$ and thickness $h>2w$ are expected in all currently discussed advanced gravitational-wave interferometers due to considerations of optical losses and mirror thermal noise. Under these conditions, we assume that the temperature and elastic distortions in a finite mirror can be approximated by the solutions for a half-infinite mirror out to radii where the intensity of the light beam becomes negligible, $\sim r\geq 2w$. We have compared Hello and Vinet for gravitational-wave mirrors and reflective beam splitters of silicon, sapphire, and fused silica to our formalism. Over the range $r<2w$, the two theories differ by less than 11% in the worst case. Figure 2 compares the two theories for different materials and optic sizes. For the case described in our experiment, where $a=12.7$ mm, $w=1.1$ mm, and the substrate is BK-7, the two theories differ by $\sim 0.3\%$. For this paper, we have used our simplified theory and believe that for studying gravitational-wave detector design, when somewhat more accuracy than is obtainable with the approach of Winkler *et al.*[13,14] is required, the simpler expressions shown here may be more convenient than the exact expressions of Hello and Vinet.

Our model uses the temperature profile in the half-infinite optic to estimate the distortions in a finite-sized mirror. Normalizing the temperatures to a characteristic value,

$$T_c=\frac{2\epsilon P}{\pi w\kappa}, \tag{4}$$

according to $\bar{T}=T/T_c$, and expressing the spatial dimensions in terms of the laser beam waist w as $\bar{r}=r/w$ and

$\bar{z}=z/w$, the boundary condition for the front face given in Eq. (2) can be written

$$-\frac{\partial \bar{T}}{\partial \bar{z}}+\frac{1}{\bar{l}_{\mathrm{th}}}\bar{T}=\exp(-2\bar{r}^2), \tag{5}$$

where $l_{\mathrm{th}}=w\bar{l}_{\mathrm{th}}=\kappa/(4\sigma' T_{\mathrm{ext}}^3)$ characterizes the relative importance of radiation versus conduction for removing heat from the illuminated region and is the only parameter in the solution for the thermal field. Appendix A shows that for a half-infinite mirror with a radiative boundary condition on the reflective surface, which is also absorbing a fraction of the laser light, the dimensionless temperature can be written

$$\bar{T}(\bar{r},\bar{z})=\frac{1}{4}\int_0^\infty \mathrm{d}k\frac{\exp[-k^2/8-k(\bar{z}+\bar{h}/2)]J_0(k\bar{r})}{1+(k\bar{l}_{\mathrm{th}})^{-1}}, \tag{6}$$

where, in this case, k is a dummy variable. For an ambient temperature of 300 K, fused silica with an emissivity of 0.5 such that $\sigma'=0.5\sigma=2.8\times10^{-8}\ \mathrm{W\,m^{-2}\,K^{-4}}$, the thermal length scale is $l_{\mathrm{th}}=0.46$ m, while in sapphire, it is $l_{\mathrm{th}}=11$ m, and in silicon, it is $l_{\mathrm{th}}=47$ m. With a beam radius of $w=3$ cm, we have $\bar{l}_{\mathrm{th}}=15$, $\bar{l}_{\mathrm{th}}=360$, and $\bar{l}_{\mathrm{th}}=1540$ for fused silica, sapphire, and silicon, respectively.

As shown in Appendix B, the temperature field of Eq. (6) can be used to calculate the thermoelastic surface deformations in both the r and the z directions using the relations for the radial and longitudinal displacements of the surface of the mass, $u_r(r)$ and $u_z(r)$, from Hello and Vinet,[16] which express the thermoelastic distortions in terms of the temperature field. It is convenient to normalize these displacements to a characteristic displacement,

$$u_c=\frac{2\alpha\epsilon P}{\pi\kappa}(1+\nu), \tag{7}$$

so that $u_r(r,z)=u_c\bar{u}_r(r,z)$ and $u_z(r,z)=u_c\bar{u}_z(r,z)$. When the radiative contribution can be neglected ($\bar{l}_{\mathrm{th}}\gg1$), universal functions result

$$\bar{u}_z(\bar{r})\approx\frac{1}{8}[E_1(2\bar{r}^2)+\gamma+\ln(2\bar{r}^2)],$$

$$\bar{u}_r(\bar{r})\approx\sqrt{\frac{\pi}{16}}\bar{r}e^{-\bar{r}^2}[I_0(\bar{r}^2)+I_1(\bar{r}^2)], \tag{8}$$

where γ is Euler's constant, E_1 is the exponential integral function, and I_n are the modified Bessel functions of order n. These expressions are adequate to analyze the experimental results presented in this paper, where a 1.1 mm heating beam on a BK-7 substrate corresponds to $\bar{l}_{\mathrm{th}}=335$. More accurate expressions valid for small $\bar{l}_{\mathrm{th}}$ can be found in Appendix B.

4. GRATING ILLUMINATED WITH A PARTIALLY ABSORBED GAUSSIAN BEAM

A diffraction grating with two real orders is functionally equivalent to a beam splitter, without requiring transmission through the substrate. Large, low-loss dielectric gratings capable of handling high power have been demonstrated, for example, at Lawrence Livermore National Laboratory[17] for stretching and compressing high-energy laser pulses. Several effects must be addressed before a grating can be considered for use as a diffractive beam splitter in a gravitational-wave interferometer.[10] The wavelength dependence of the diffraction angle couples laser frequency noise to beam pointing fluctuations; the spatial profile of the diffracted beam is in general elliptical; and thermoelastic deformation of the substrate affects the diffracted beam differently than the reflected beam. As discussed in Ref. 10, using the grating near the Littrow configuration reduces the ellipticity of the diffracted beam, and the dispersion in the grating can be compensated for by using an additional grating or by double passing the grating to null the dispersion. The wavefront distortions on the reflected and diffracted beams imposed by the thermoelastic distortion of the grating caused by heating when a small fraction of the Gaussian light beam is absorbed in the grating surface are analyzed in Appendix C. For the undiffracted beam, only the axial distortions come into play, and the wavefront in the observation plane is written

$$\varphi_{\mathrm{Undiff}}(x_O,z_O)=\frac{2k}{\cos(\theta)}u_z\left[\frac{x_O}{\cos(\theta)},z_O\right]. \tag{9}$$

For the diffracted beam, both the radial and the axial distortions are important, and the result is

$$\varphi_{\mathrm{Diff}}(x_O)=k_g^{(0)}u_r\left[\frac{x_O}{\cos(\phi)},0\right]+k\left(\frac{1}{\cos(\theta)}+\frac{1}{\cos(\phi)}\right)\times u_z\left[\frac{x_O}{\cos(\phi)},0\right]. \tag{10}$$

The coordinates are defined in Fig. 1, and k and $k_g^{(0)}$ are the wavenumbers of the incident radiation and unheated grating, respectively. For the diffracted beam, we plot the distortion along x, the direction most affected by the distortion of the grating. Examples of the wavefront gradient calculated from these expressions are shown in Fig. 6.

5. EXPERIMENT

Figure 3 shows the experimental setup used to study the effects of laser beam heating on both the diffracted and the reflected beams from a grating. A gold-coated reflection grating with a pitch of $d=568$ nm on a BK-7 substrate (diameter 24.5 mm and thickness 10 mm) was illuminated with the output of an argon-ion laser oscillating at both 514 and 488 nm. The beam was normally incident and had a spot size of 1.1 mm at the grating. By measuring the incident, reflected, and diffracted beam powers, the absorbed fraction of the incident power was estimated to be 52%. No light was visible in transmission through the BK-7 substrate. The ion-laser power at the grating was controlled with a wave plate and a polarizer. The distorted grating was then probed using a 10 mW, 633 nm helium–neon laser beam that was expanded to a spot size of $w_{\mathrm{probe}}=2$ mm at the grating with an angle of incidence of 30°. The gradient of the wavefronts of the diffracted

and the reflected beams were then measured using a Shack–Hartmann wavefront sensor[18,19] at several different incident heating beam powers. Notice that for experimental convenience, we use two beams, one to heat and distort the grating and the other to probe the distortions.

The Shack–Hartmann wavefront sensor operates by passing the beam to be measured through a two-dimensional array of microlenses and from there onto a two-dimensional detector array. The sensor measures the gradient of the wavefront of the light beam by determining the position of the spot each microlens focuses onto the detector array and comparing the spot positions to those of a reference measurement. In this experiment, the reference was obtained by measuring the positions of the focused probe beam spots when the grating was not illuminated with the heating beam. The heating beam was then turned on, set to a particular power, the positions of the focused spots were recorded, and from the changes in

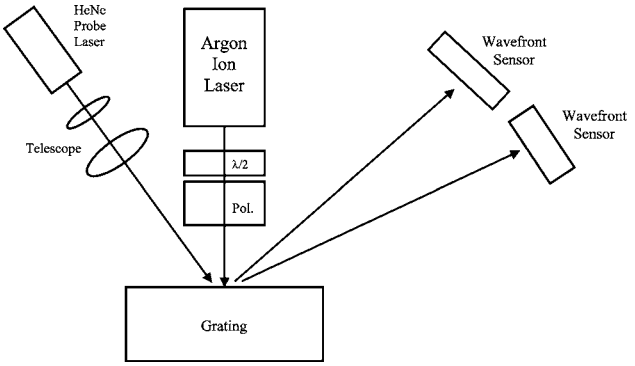

Fig. 3. Grating is illuminated with a heating beam whose power can be varied using a wave plate and a polarizer. The surface distortions are probed using a helium–neon laser and a Shack–Hartmann wavefront sensor. The probe beam is incident at 30° to the grating surface normal.

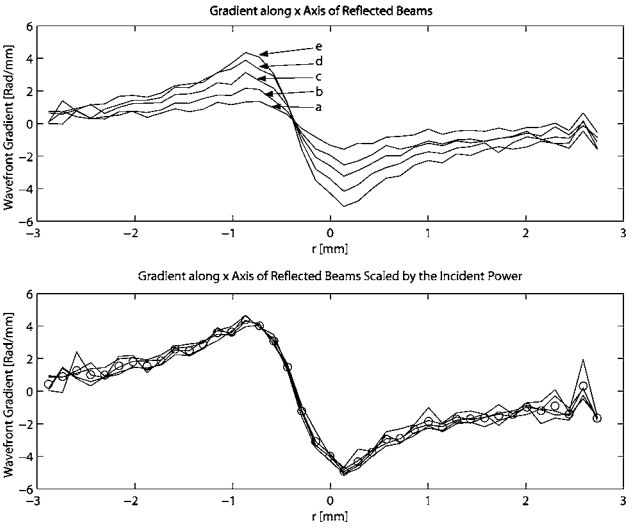

Fig. 4. Five measured wavefront gradients of the reflected beam (upper figure) at the wavefront sensor. The curves corresponding to (a) 106 mW, (b) 158 mW, (c) 212 mW, (d) 265 mW, and (e) 315 mW of incident power. Each of the data sets in the top figure is scaled to 315 mW in the lower figure. Because the distortion is a linear function of absorbed power, the data sets can all be scaled to the same power and then averaged, which is the plot labeled (◦).

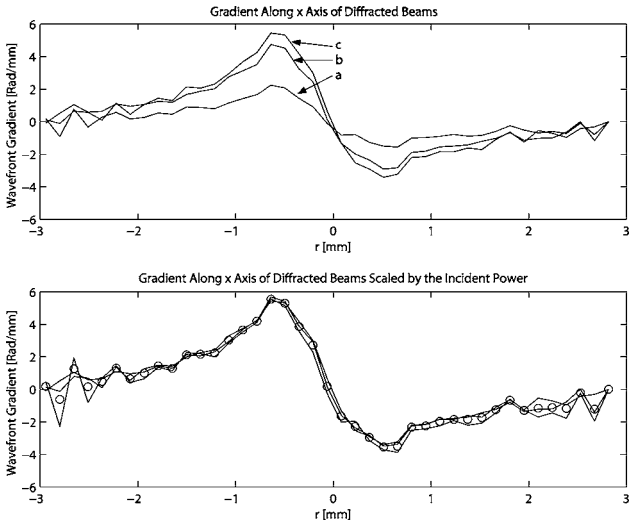

Fig. 5. Three measured wavefront gradients of the diffracted beam (upper figure) at the wavefront sensor. The curves correspond to (a) 125 mW, (b) 259 mW, and (c) 310 mW of incident power. Each of the data sets is scaled to 310 mW in the lower figure, and the scaled data sets are then averaged, which is the plot labeled (◦).

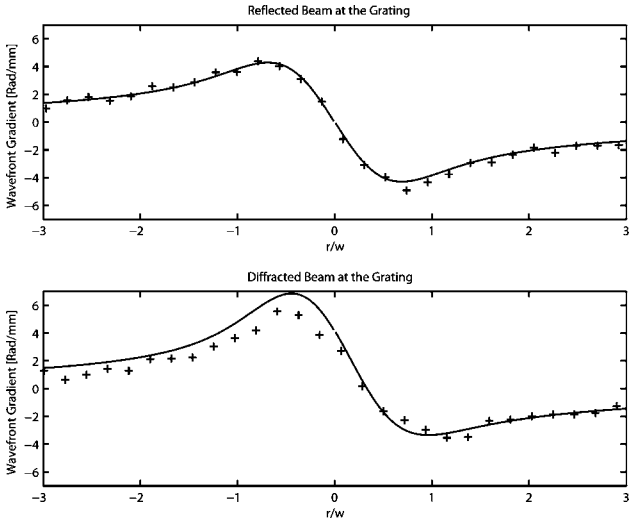

Fig. 6. Comparison of the averaged wavefront gradient of the reflected beam (top) and the diffracted beam (bottom) to the simplified theory. These two comparisons use no free parameters.

the spot positions, the gradient of the phase front at the microlens array was estimated. Measurements of both the reflected and the diffracted beams were made using the wavefront sensor at several different heating beam powers. Figure 4 (top) shows the measured phase gradients of the reflected beams at incident powers of 106, 158, 212, 265, and 315 mW while Fig. 4 (bottom) shows all of the data sets scaled linearly to an incident power of 315 mW along with the average of these scaled data sets. It is this averaged data that we will compare to theory. Figure 5 (top) shows the measured phase gradients of the diffracted beams at powers of 125, 259, and 310 mW while Fig. 5 (bottom) shows all of the data sets scaled to 310 mW and the average of these scaled data sets. Again this scaled and averaged data will be compared to theory.

We compare, in Fig. 6, the averaged data for the re-

flected and diffracted beams with Eqs. (9) and (10), using no free parameters. We see good agreement between the calculated and experimental wavefront gradients. Note that the reflected beam is only distorted by the axial deformations while the diffracted beam distortions are influenced by both the radial and the axial grating distortions because the pitch of the grating is no longer a constant across the grating surface. These distortions are even and odd with respect to the origin of the beam, respectively, so that their sum results in a slight asymmetry in the total wavefront distortion. What discrepancy there is between data and theory can be explained by our inability to precisely control the boundary conditions of the optic.

6. IMPLICATIONS FOR HIGH-POWER INTERFEROMETRY

The geometrical arrangement of the experiment described here in which the heating beam is at normal incidence to the grating and a separate probe beam is used is different from the geometry that will be used in a gravitational-wave interferometer where the incident and heating beams are the same. However, an estimate of the wavefront distortions that would be obtained in a gravitational-wave interferometer can be obtained for the case in which the incident and diffracted beam are near normal incidence. The rms wavefront distortion along the x_0 axis for the diffracted beam is written

$$\delta\varphi_{\mathrm{rms}}^{\mathrm{Diff}} = \left[\sqrt{\frac{2}{\pi w^2}} \int_{-\infty}^{+\infty} \mathrm{d}x_0 \varphi_{\mathrm{Diff}}^2(x_O,0) e^{-2x_0^2/w^2} \right]^{1/2},$$

and a similar expression holds for the undiffracted beam. For a silicon grating and 4 cm beams at 1064 nm wavelength, the rms wavefront distortion for the diffracted beam is 2.8×10^{-3} waves per watt, and for the undiffracted beam it is 1.9×10^{-3} waves per watt. The material constants used in this estimate are listed in Table 1. Thus, even with 1 MW circulating in the interferometer arms and 1 ppm absorption in the coating, a wavefront distortion of a little over 10^{-3} waves would result.

In comparison, consider a conventional fused-silica transmissive beam splitter limited by thermal distortion due to absorption in the substrate. This estimate can be made using the well-known expression for the temperature distribution in an infinite medium heated by a Gaussian beam of $1/e^2$ radius w and with an absorption per unit length a,

$$\Delta T(r) = \frac{-aP}{4\pi\kappa} \left\{ E_1\left[2\left(\frac{r}{w}\right)^2 \right] + \gamma + \ln\left[2\left(\frac{r}{w}\right)^2 \right] \right\}.$$

The phase front distortion after passing through a substrate of thickness L, neglecting end effects, is

$$\varphi(r) = \int_0^L \mathrm{d}z \frac{2\pi}{\lambda} \frac{\mathrm{d}n}{\mathrm{d}T} \Delta T(r) = \frac{2\pi L}{\lambda} \frac{\mathrm{d}n}{\mathrm{d}T} \Delta T(r).$$

Computing the rms wavefront distortion in fused silica, we find 0.42 waves per watt of absorbed power. Thus, all else being equal, a silicon reflective beam splitter could support approximately 150 times more optical power than a fused-silica transmissive beam splitter.

Table 1. Material Properties

Property	BK-7	Silicon	Fused Silica	Sapphire
α [1/K]	7.1×10^{-6}	2.6×10^{-6}	0.54×10^{-6}	5.1×10^{-6}
κ [w/m K]	1.114	141.2	1.38	33
ν	0.206	0.2154	0.17	0.23
$\mathrm{d}n/\mathrm{d}T$	10^{-6}	160×10^{-6}	1.35×10^{-5}	10^{-5}

7. CONCLUSION

We have measured wavefront distortions induced on Gaussian beams reflected and diffracted from a grating thermally loaded by partial absorption of a Gaussian laser beam. The results are in good accord with simple theoretical expressions for the wavefront distortions. Our expressions for the radial and axial distortion of a grating or mirror experiencing surface absorption of a Gaussian beam agree to a few percent with Hello and Vinet when $a>10w$. For mirrors and gratings appropriate for gravitational wave detectors where $a\approx2.5w$, the expressions agree to within 13.7%.

The expressions show that in a gravitational-wave detector, the diffracted beam can undergo distortions 50% larger than those experienced by the reflected beam, but that these are still several orders of magnitude smaller than would be experienced in a transmissive optic under similar conditions.

APPENDIX A: ANALYTICAL EXPRESSION FOR THE TEMPERATURE FIELD IN A HALF-INFINITE CYLINDER HEATED AT ITS SURFACE BY A GAUSSIAN LIGHT BEAM

After casting the heat diffusion equation in a form where we have nondimensionalized the radius r and the axial coordinate z to the laser beam spot size w and the temperature to a characteristic center–edge temperature rise T_c, i.e., $\bar{r}=r/w$, $\bar{z}=z/w$, $\bar{T}=T/T_c$, where

$$T_c = \frac{2\epsilon P}{\pi w \kappa}, \tag{A1}$$

the heat diffusion equation for the geometry shown in Fig. 1 becomes

$$\nabla^2 \bar{T}(\bar{r},\bar{z}) = 0, \tag{A2}$$

and the boundary conditions are $\bar{T}(\bar{r}\to\infty,\bar{z})=0$, $\bar{T}(\bar{r},\bar{z}\to+\infty)=0$, and

$$-\frac{\partial \bar{T}(\bar{r},-\bar{h}/2)}{\partial \bar{z}} + \frac{1}{\bar{l}_{\mathrm{th}}} \bar{T}(\bar{r},-\bar{h}/2) = e^{-2\bar{r}^2}, \tag{A3}$$

where a characteristic thermal length l_{th} is defined as

$$l_{\mathrm{th}} = \frac{\kappa}{4\sigma' T_{\mathrm{ext}}^3}, \tag{A4}$$

and $\bar{l}_{\mathrm{th}}=l_{\mathrm{th}}/w$.

Assuming cylindrical symmetry, Eq. (A2) takes the form,

$$\frac{\partial^2 \bar{T}(\bar{r},\bar{z})}{\partial \bar{r}^2} + \frac{1}{\bar{r}}\frac{\partial \bar{T}(\bar{r},\bar{z})}{\partial \bar{r}} + \frac{\partial^2 \bar{T}(\bar{r},\bar{z})}{\partial \bar{z}^2} = 0. \tag{A5}$$

The solutions of this equation vanishing at infinity are of the form $\exp(-kz)J_0(kr)$, where for an infinite radial extent, the choice of k is unconstrained. To meet the boundary condition at $z=-h/2$, we construct a superposition of the allowed solutions:

$$T(\bar{r},\bar{z}) = \int_0^\infty \mathrm{d}k A(k) e^{-(\bar{z}+\bar{h}/2)k} J_0(\bar{r}k), \tag{A6}$$

We now determine $A(k)$ by substituting the solution (A6) into the boundary condition (A3), interchanging the order of integration and differentiation, evaluating the expression at $\bar{z}=-\bar{h}/2$, multiplying both sides by $rJ_0(k'r)$, and using the orthogonality relation for the Bessel functions. We find

$$A(k')(1 + 1/k\bar{l}_{\mathrm{th}}) = \int_0^\infty \mathrm{d}r e^{-2\bar{r}^2} r J_0(rk'). \tag{A7}$$

Noting that the integral can be evaluated as $\exp(-k^2/8)/4$, we can solve for $A(k)$ and, substituting back into Eq. (A6) obtain the desired solution,

$$\bar{T}(\bar{r},\bar{z}) = \frac{1}{4}\int_0^\infty \mathrm{d}k \frac{e^{-k^2/8} e^{-(\bar{z}+\bar{h}/2)k} J_0(k\bar{r})}{(1 + 1/k\bar{l}_{\mathrm{th}})}. \tag{A8}$$

APPENDIX B: THERMOELASTIC DISTORTIONS IN A GRATING HEATED AT ITS SURFACE BY A GAUSSIAN LIGHT BEAM

Given a cylindrically symmetric temperature field $T(r,z)$, an integral expression for the radial displacement $u_r(r,z)$ due to thermal expansion in a right circular cylinder is, from Hello and Vinet,[15]

$$u_r(r,z) = \frac{\nu_T}{2(\lambda+\mu)}\frac{1}{r}\int_0^r T(r',z) r' \mathrm{d}r', \tag{B1}$$

where $\nu_T=\alpha(3\lambda+2\mu)$ is the stress temperature modulus and λ and μ are the Lame coefficients. Similarly, an expression for the axial displacement u_z is

$$u_z(r,z) = \frac{\nu_T}{2(\lambda+\mu)}\left[\int_{-\bar{h}/2}^{z} T(r,z')\mathrm{d}z' - \int_0^r \frac{\mathrm{d}r'}{r'}\int_0^{r'} \frac{\partial T(r'',-h/2)}{\partial z} r''\mathrm{d}r'' + C\right]. \tag{B2}$$

Using a characteristic displacement u_c, Eqs. (B1) and (B2) can be written for the normalized displacements $\bar{u}_z = u_z/\bar{u}_c$ and $\bar{u}_r = u_r/u_c$,

$$\bar{u}_r(\bar{r},\bar{z}) = \frac{1}{\bar{r}}\int_0^{\bar{r}} \bar{T}(\bar{r}',\bar{z})\bar{r}'\mathrm{d}\bar{r}', \tag{B3}$$

$$\bar{u}_z(\bar{r},-\bar{h}/2) = -\int_0^{\bar{r}}\frac{\mathrm{d}\bar{r}'}{\bar{r}'}\int_0^{\bar{r}'}\frac{\partial \bar{T}(\bar{r}'',-\bar{h}/2)}{\partial \bar{z}}\bar{r}''\mathrm{d}\bar{r}'', \tag{B4}$$

where $u_c \equiv \nu_T w T_c/2(\lambda+\mu) = \alpha(3\lambda+2\mu)/\pi(\lambda+\mu)\,\epsilon P/\kappa = (2\alpha\epsilon P/\pi\kappa)(1+\nu)$, and we have neglected terms in the displacement that are independent of r since these do not contribute to the distortion of the wavefront.

1. Axial Distortion

Consider first the axial distortion, u_z. Using Eq. (A3) for the boundary condition in the plane defined by $z=-h/2$, i.e., $\bar{z}=-(h/2w)$, in Eq. (B4), we find

$$\bar{u}_z(\bar{r},-\bar{h}/2) = \bar{u}_{z0}(\bar{r}) + \bar{u}_{z1}(\bar{r})/\bar{l}_{\mathrm{th}}, \tag{B5}$$

where

$$\bar{u}_{z0}(\bar{r}) = \int_0^{\bar{r}}\frac{\mathrm{d}\bar{r}'}{\bar{r}'}\int_0^{\bar{r}'} e^{-2\bar{r}''^2}\bar{r}''\mathrm{d}\bar{r}'',$$

$$\bar{u}_{z1}(\bar{r}) = \int_0^{\bar{r}}\frac{\mathrm{d}\bar{r}'}{\bar{r}'}\int_0^{\bar{r}} \bar{T}(\bar{r}'',-\bar{h}/2)\bar{r}''\mathrm{d}\bar{r}''.$$

After integrating the inner integral in the expression for u_{z0}, the outer integral is a standard form resulting in

$$\bar{u}_{z0}(\bar{r}) = \frac{1}{8}\left[E_1(2\bar{r}^2) + \gamma + \ln(2\bar{r}^2)\right], \tag{B6}$$

where E_1 is the exponential integral function[20] and γ is Euler's constant.

Evaluation of $\bar{u}_{z1}$, is somewhat more complex. Inserting the expression (A8) for the temperature field into Eq. (B5) for $\bar{u}_{z1}$, and reversing the order of integration, we obtain

$$\bar{u}_{z1}(\bar{r},\bar{l}_{\mathrm{th}}) = \frac{1}{4}\int_0^\infty \mathrm{d}k \frac{e^{-k^2/8}}{1+1/(k\bar{l}_{\mathrm{th}})}\int_0^{\bar{r}}\frac{\mathrm{d}\bar{r}'}{\bar{r}'}\int_0^{\bar{r}'} J_0(k\bar{r}'')\bar{r}''\mathrm{d}\bar{r}''$$

$$= \frac{1}{4}\int_0^{\bar{r}}\mathrm{d}\bar{r}'\int_0^\infty \mathrm{d}k \frac{e^{-k^2/8}}{k+1/\bar{l}_{\mathrm{th}}} J_1(k\bar{r}'), \tag{B7}$$

where the second form follows from a standard indefinite integral of the Bessel functions. It is not possible to integrate Eq. (B7) analytically except in the limit $\bar{l}_{\mathrm{th}}\to\infty$. Noting that $\bar{l}_{\mathrm{th}}$ is generally large, and one factor of $1/\bar{l}_{\mathrm{th}}$ already precedes $\bar{u}_{z1}$ in Eq. (B5), we consider this limit. The results are seen to be in good agreement with those obtained using numerical integration. Evaluating Eq. (B7) in this limit, we obtain

$$\bar{u}_{z1}(\bar{r}) = \frac{1}{8}\int_0^{\bar{r}}\mathrm{d}r' r'\int_0^\infty \mathrm{d}k e^{-k^2/8}[J_0(kr') + J_2(kr')]$$

$$= \frac{\sqrt{2\pi}}{8}\int_0^{\bar{r}}\mathrm{d}r' r' e^{-r'^2}[I_0(r'^2) + I_2(r'^2)]$$

$$= \frac{\sqrt{\pi/2}}{8}\{2r^2 e^{-r^2}[I_0(r^2) + I_2(r^2)] + [e^{-r^2}I_0(r^2) - 1]\}, \tag{B8}$$

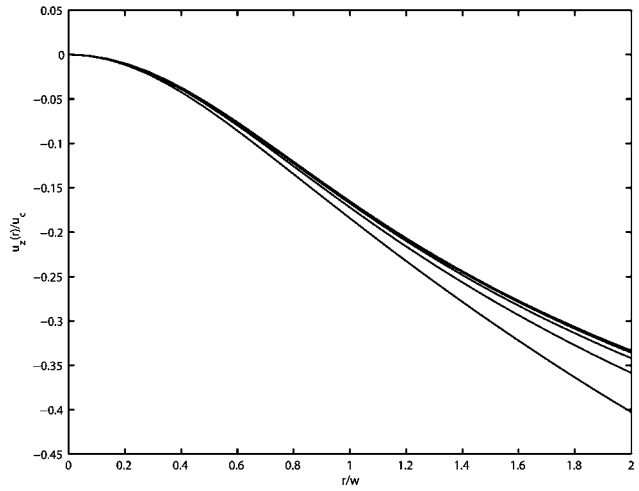

Fig. 7. Axial surface deformation of a cylindrical substrate illuminated with a Gaussian beam plotted using Eq. (B9). The axial deformation causes a distortion on the surface thus changing the radius of curvature of the optic. The magnitude of the deformation is normalized to the characteristic displacement of the substrate material given by Eq. (7). $\{l_{\mathrm{th}}=4$ (bottom curve), 10.6, 28.2, 75.2, and 200 (top curve)$\}$. As l_{th} becomes large, the curves approach a universal function given by Eq. (8). The radial coordinate is in units of the laser spot size, and the axial distortion is in units of the characteristic displacement u_c.

where the first form makes use of a Bessel function recursion relation, and the second and third forms are tabulated definite and indefinite integrals, respectively. Finally, inserting Eq. (6) and (8) into Eq. (B5), we arrive at the axial deformation to leading order in $1/\bar{l}_{\mathrm{th}}$,

$$\bar{u}_{\bar{z}}(\bar{r}) \approx \frac{1}{8}[E_1(2\bar{r}^2)+\gamma+\ln(2\bar{r}^2)] - \frac{1}{\bar{l}_{\mathrm{th}}}\frac{\sqrt{\pi/2}}{8} \times\{2\bar{r}^2 e^{-\bar{r}^2}[I_0(\bar{r}^2)+I_2(\bar{r}^2)]+[e^{-\bar{r}^2}I_0(\bar{r}^2)-1]\}, \tag{B9}$$

which is plotted in Fig. 7 for various values of $\bar{l}_{\mathrm{th}}$. Empirically, we have found that the same asymptotic accuracy for large $\bar{l}_{\mathrm{th}}$ is obtained along with improved accuracy for moderate values of $\bar{l}_{\mathrm{th}}$ by replacing $\bar{l}_{\mathrm{th}}\rightarrow\bar{l}_{\mathrm{th}}+1$ in Eq. (B9).

2. Radial Distortion

The analysis of the radial distortion begins with Eq. (B1) into which we again insert the integral expression for the temperature field, Eq. (A8), to obtain

$$\bar{u}_r(\bar{r},\bar{l}_{\mathrm{th}}) = \frac{1}{\bar{r}}\int_0^{\bar{r}} \mathrm{d}r' r' \frac{1}{4}\int_0^{\infty} \mathrm{d}k \frac{e^{-k^2/8}J_0(kr')}{1+1/(k\bar{l}_{\mathrm{th}})} = \frac{1}{4}\int_0^{\infty} \mathrm{d}k e^{-k^2/8}\frac{J_1(kr')}{k+1/\bar{l}_{\mathrm{th}}}, \tag{B10}$$

where the second form is obtained by interchanging the order of integration and applying a standard Bessel function indefinite integral. In the limit $\bar{l}_{\mathrm{th}}\rightarrow\infty$, Eq. (B10) can be evaluated analytically:

$$\bar{u}_r(\bar{r},\bar{l}_{\mathrm{th}}\rightarrow\infty) = \bar{u}_{r,0}(\bar{r}) = \frac{1}{4}\int_0^{\infty} \mathrm{d}k e^{-k^2/8}\frac{J_1(kr')}{k} = \frac{\sqrt{\pi/2}}{4}\bar{r}e^{-\bar{r}^2}[I_0(\bar{r}^2)+I_1(\bar{r}^2)]. \tag{B11}$$

For large values of $\bar{l}_{\mathrm{th}}$ the universal ($\bar{l}_{\mathrm{th}}$ independent) function $\bar{u}_{r,0}(\bar{r})$ is adequate to describe the in-plane displacements. Corrections dependent on $\bar{l}_{\mathrm{th}}$ can become significant for large beams on low thermal conductivity materials like fused silica. To address these cases, we can write Eq. (B10) as

$$\bar{u}_r(\bar{r},\bar{l}_{\mathrm{th}}) = \bar{u}_{r0}(\bar{r}) - U_r(\bar{r},\bar{l}_{\mathrm{th}}), \tag{B12}$$

where

$$U_r(\bar{r},\bar{l}_{\mathrm{th}}) = \frac{1}{4}\int_0^{\infty} \mathrm{d}k e^{-k^2/8}\frac{J_1(k\bar{r})}{k(1+k\bar{l}_{\mathrm{th}})}. \tag{B13}$$

It is not possible to integrate Eq. (B13) in closed form. Approximation is subtle, due to leading behavior that goes as $\bar{r}\ln(\bar{l}_{\mathrm{th}})$. To separate out this term explicitly, we write, Eq. (B13) as

$$U_r(\bar{r},\bar{l}_{\mathrm{th}}) = \bar{u}_{r1}(\bar{r},\bar{l}_{\mathrm{th}})/\bar{l}_{\mathrm{th}} + \frac{\bar{r}}{2}P(\bar{l}_{\mathrm{th}}), \tag{B14}$$

where

$$\bar{u}_{r1}(\bar{r},\bar{l}_{\mathrm{th}}) = \frac{1}{4}\int_0^{\infty} \mathrm{d}k e^{-k^2/8}\frac{J_1(k\bar{r})/k-\bar{r}/2}{k+1/\bar{l}_{\mathrm{th}}}, \tag{B15}$$

$$P(\bar{l}_{\mathrm{th}}) = \frac{1}{4}\int_0^{\infty} \mathrm{d}k e^{-k^2/8}\frac{1}{1+k\bar{l}_{\mathrm{th}}}. \tag{B16}$$

Up to this point, the analysis has been exact, but Eq. (B15) is not integrable in closed form. As we again are interested primarily in the large $\bar{l}_{\mathrm{th}}$ limit, and a factor $1/\bar{l}_{\mathrm{th}}$ has already been explicitly removed from u_{r1}, we evaluate Eq. (B5) in the limit $\bar{l}_{\mathrm{th}}\rightarrow\infty$:

$$\bar{u}_{r1}(\bar{r},\bar{l}_{\mathrm{th}}\rightarrow\infty) = \bar{u}_{r1}(\bar{r}) = \frac{1}{4}\int_0^{\infty} \mathrm{d}k e^{-k^2/8}\frac{J_1(k\bar{r})/k-\bar{r}/2}{k+1/\bar{l}_{\mathrm{th}}} = -\{1-e^{-2\bar{r}^2}+2\bar{r}[\gamma-1+E_1(2\bar{r}^2) + \ln(2\bar{r}^2)]\}\Big/32\bar{r}. \tag{B17}$$

We have found only the leading behavior necessary to describe cases of practical importance. P is of less importance, as we generally are not interested in the simple tilt of the wavefront represented by the linear-in-r dependence. For completeness, we note that Eq. (B6) can be integrated exactly to yield

$$P(\bar{l}_{\mathrm{th}}) = -\bar{l}_{\mathrm{th}}be^{-b}(i\pi\,\mathrm{erf}(i\sqrt{b})+\mathrm{Ei}(b)) \approx b[\sqrt{\pi/2}-\bar{l}_{\mathrm{th}}(\ln b+\gamma)], \tag{B18}$$

where $b=1/(8\bar{l}_{\mathrm{th}}^2)$ and Ei is the second exponential integral function.[20]

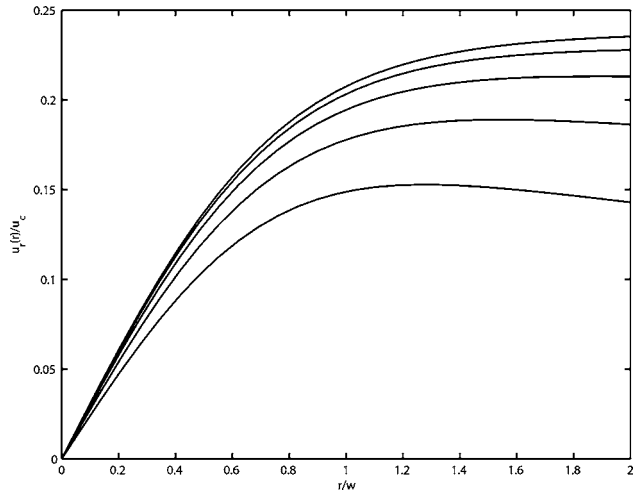

Fig. 8. Radial surface deformation of a cylindrical substrate heated by absorption of a Gaussian beam, calculated with Eq. (B19). The radial deformation is only relevant when the optic is used as a grating because it causes the spacing of the grating grooves to change nonuniformly. The magnitude of the deformation is normalized to the characteristic displacement of the substrate material given by Eq. (7). $\{l_{\mathrm{th}}=4$ (bottom curve), 10.6, 28.2, 75.2, and 200 (top curve)$\}$. As l_{th} becomes large, the curves approach a universal function shown by Eq. (8). The radial coordinate is in units of the laser spot size.

The complete approximation to the radial distortion is then given by combining Eqs. (B11), (B12), (B14), and (B17) to obtain

$$\bar{u}_r(\bar{r},\bar{l}_{\mathrm{th}}) = \frac{\sqrt{\pi/2}}{4}\bar{r}e^{-\bar{r}^2}[I_0(\bar{r}^2)+I_1(\bar{r}^2)] + 1 - e^{-2\bar{r}^2} + 2\bar{r}^2[\gamma - 1 + E_1(2\bar{r}^2) + \ln(2\bar{r}^2)]\Big/(32\bar{r}\bar{l}_{\mathrm{th}}) - \frac{\bar{r}}{2}P(\bar{l}_{\mathrm{th}}), \tag{B19}$$

where we have not inserted the result for P as the wavefront tilt is rarely of importance in practice. This function is plotted in Fig. 8 for several values of $\bar{l}_{\mathrm{th}}$. As was the case for the axial displacement in Eq. (B19), we find empirically that the same asymptotic accuracy for large $\bar{l}_{\mathrm{th}}$ is obtained along with improved accuracy for moderate values of $\bar{l}_{\mathrm{th}}$ by replacing $\bar{l}_{\mathrm{th}} \rightarrow \bar{l}_{\mathrm{th}}+1$ in Eq. (B19).

APPENDIX C: WAVEFRONT DISTORTIONS IMPOSED ON GAUSSIAN LIGHT BEAMS REFLECTED OR DIFFRACTED FROM A GRATING UNDERGOING THERMOELASTIC DISTORTIONS

In this appendix, we use the Huygens integral to compute the wavefront distortions of the reflected and diffracted beams from a grating that is being heated by a second Gaussian beam partially absorbed at the grating surface. The Huygens integral is used to propagate the field from the grating surface to the observation plane. The phase front of the light beams just above the surface of the grating have contributions from three sources. First, the undistorted grating, second, the axial displacement of the grating surface $u_z(r)$, and third, the in-plane distortion $u_r(r)$, which causes the grating pitch to vary with position. The reflected beam is only affected by the axial distortion while the diffracted beam is affected by both the axial and the radial distortions.

The source plane (x_s,z_s) is contained in the grating surface where z_s is parallel to the grating grooves and x_s is perpendicular to the grating grooves while the coordinate y_s is perpendicular to the grating surface as shown in Fig. 1. The incident Gaussian beam propagates in the (x_s,y_s) plane at an angle θ to the y_s axis while the diffracted beam propagates in the (x_s,y_s) plane at an angle ϕ to the y_s axis. The observation plane (x_o,z_o) is perpendicular to the diffracted beam direction. The Huygens integral for the diffracted field in the observation plane is written

$$E(x_o,z_o) = \frac{i}{\lambda}\int_{-\infty}^{+\infty}\mathrm{d}x_s\int_{-\infty}^{+\infty}\mathrm{d}z_s E(x_s,z_s)\frac{e^{ik\rho(x_s,z_s;x_o z_o)}}{\rho(x_s,z_s;x_o,z_o)}e^{i\varphi(x_s,z_s)}, \tag{C1}$$

where the integration is carried out over the grating surface. In this equation, $\rho(x_s,z_s;x_o,z_o)$ is the distance from any point in the source plane to any point in the observation plane. $\varphi(x_s,z_s)$ is the phase shift impressed on the light beam by the sinusoidal phase grating of amplitude $\delta\varphi_g$ and the axial and radial thermoelastic deformations and is given by

$$\varphi(x_s,z_s) = kA(\theta,\phi)u_z(x_s,z_s) + \delta\varphi_g A(\theta,\phi)\cos[\Theta(x_s,z_s)],$$

$$A(\theta,\phi) = \left[\frac{1}{\cos(\theta)} + \frac{1}{\cos(\phi)}\right]. \tag{C2}$$

The accumulated phase in the cosine term contains both the undistorted grating, and the distortions to the grating as parameterized by the strain $\mathrm{d}u/\mathrm{d}x$,

$$\Theta = \int \vec{k}_g(\vec{r})\cdot\mathrm{d}\vec{s} = \int k_g^{(0)}\left[1 - \frac{\mathrm{d}u_x}{\mathrm{d}x}\right]\hat{x}\cdot\hat{r}\,\mathrm{d}r = k_g^{(0)}\int\left[1 - \frac{\mathrm{d}u_x}{\mathrm{d}x}\right]\cos(\alpha)\mathrm{d}r = k_g^{(0)}x - \vartheta(x,z)$$

$$\vartheta(x,z) = -k_g^{(0)}\frac{x^3}{(x^2+z^2)^{3/2}}u_r(r) - k_g^{(0)}\frac{xz^2}{(x^2+z^2)^{3/2}}\int\frac{u_r}{r}\mathrm{d}r, \tag{C3}$$

where $k_g^{(0)}\hat{x}$ is the unperturbed grating k vector. Explicitly writing out the terms corresponding to the reflected beam and the first two diffracted orders for low diffraction efficiency,

$$\exp[i\varphi(x_s,z_s)] \approx \exp\{ikAu_z(x_s,z_s)\}\times\left\{1 + i\frac{\delta\varphi_g A}{2}\{\exp[ik_g x - i\vartheta(x_s,z_s)] + \exp[-ik_g x_s + i\vartheta(x_s,z_s)]\}\right\}. \tag{C4}$$

The first term in the brackets corresponds to the reflected beam, and the second and third terms correspond to the first +1 and −1 diffracted orders, respectively. Writing the Huygens integral for the −1 diffracted order, grouping factors not functions of the integration variable as $B(z)$, observing that the argument of the second exponential is zero as a consequence of the grating equation and separating the slowly and rapidly varying factors yields

$$E(x_o,z_o) = B(z_o)\int_{-\infty}^{+\infty} \mathrm{d}z_s \exp(-z_s^2/w^2)\exp[ikAu_z(x_s,z_s)] \times \exp[iS_1(z_o,z_s)]\int_{-\infty}^{+\infty} \mathrm{d}x_s \exp[i\vartheta(x_s,z_s)] \times \exp\left[-\frac{\cos^2(\theta)}{w^2}x_s^2\right]\exp[iS_2(z_o,z_s)],$$

where

$$B(z_o) = -\frac{E_o\delta\varphi_g A(\theta,\phi)}{2\lambda L}\exp\left[ikL + ik\frac{x_o^2}{2L}\right],$$

$$S_1(z_o,z_s) = k\frac{(z_o-z_s)^2}{2L},$$

$$S_2(z_o,z_s) = k\left[\cos(\phi)\left(\frac{x_o}{L}\right)x_s + \frac{\cos^2(\phi)}{2L}x_s^2\right]. \quad \text{(C5)}$$

The first two exponential factors in each integrand are slowly varying functions of the integration variables while the third exponential factor varies rapidly everywhere except near their turning points. The major contributions to the integrals come from the regions near the turning points that are at $z_s^{(0)}=z_o$ and $x_s^o=-x_o/\cos(\phi)$. Using the method of stationary phase to evaluate Eq. (C5), we find for the electric field at $(x_o,z_o=0)$,

$$E(x_o) = E(x_o,z_o)|_{z_o=0} \propto \exp\left[-\frac{x_o^2}{w^2}\frac{\cos^2(\theta)}{\cos^2(\phi)}\right] \times \exp\left\{ik_g^{(0)}u_r\left(\frac{x_o}{\cos(\phi)},0\right) + ik\left[\frac{1}{\cos(\theta)}+\frac{1}{\cos(\phi)}\right] \times u_z\left(\frac{x_o}{\cos(\phi)},0\right)\right\}. \quad \text{(C6)}$$

The phase of the diffracted beam is then

$$\varphi(x_o) = k_g^{(0)}u_r\left[\frac{x_o}{\cos(\phi)},0\right] + k\left[\frac{1}{\cos(\theta)}+\frac{1}{\cos(\phi)}\right]u_z\left[\frac{x_o}{\cos(\phi)},0\right]. \quad \text{(C7)}$$

Similarly for the reflected beam,

$$E(x_o,z_o) \propto \exp\left[\left(-\frac{z_o^2}{w^2}\right)\exp\left(i\frac{2k}{\cos(\theta)}u_z\right)\left(\frac{x_o}{\cos(\theta)},z_o\right) - \frac{x_o^2}{w^2}\right], \quad \text{(C8)}$$

and the reflected beam phase is

$$\varphi(x_o,z_o) = \frac{2k}{\cos(\theta)}u_z\left[\frac{x_o}{\cos(\theta)},z_o\right]. \quad \text{(C9)}$$

Using Eq. (C7) and (C9), we can now compute the wavefront distortions for the reflected and diffracted beams from the axial and radial thermoelastic distortions.

ACKNOWLEDGMENTS

This work was supported by the National Science Foundation under grant PHY-0140297-002. Additionally, S. Traeger thanks the Alexander von Humboldt Foundation for financial support.

Corresponding author P. P. Lu's e-mail address is patlu@stanford.edu.

*Present address, San Jose State University, Science Building #235, San Jose, California 95192.

†Present address, Leiter Carl Zeiss Meditec AG, Goeschwitzer Strasse 51-52, D-07745 Jena, Germany.

‡Present address, MZA Associates Corporation, 2021 Girard Blvd. SE, #150, Albuquerque, New Mexico 87106.

**Present address, Lightconnect Inc., 35445 Dumbarton Court, Newark, California 94560.

REFERENCES

1. P. Fritschel, "The second generation LIGO [Laser Interferometer Gravitational-Wave Observatory] interferometers," in AIP Conf. Proc. **575**, 15–23 (2001).
2. K. Kuroda, M. Ohashi, S. Miyoki, D. Tatsumi, S. Sato, H. Ishizuka, M. K. Fujimoto, S. Kawamura, R. Takahashi, T. Yamazaki, K. Arai, M. Fukushima, K. Waseda, S. Telada, A. Ueda, T. Shintomi, A. Yamamoto, T. Suzuki, Y. Saito, T. Haruyama, N. Sato, K. Tsubono, K. Kawabe, M. Ando, K. I. Ueda, H. Yoneda, M. Musha, N. Mio, S. Moriwaki, A. Araya, N. Kanda, and M. E. Tobar, "Large-scale cryogenic gravitational wave telescope," Int. J. Mod. Phys. D **8**, 557–579 (1999).
3. J. Hough, "GEO-HF—a GEO Upgrade 2008+," presented at the LIGO Science Collaboration Meeting, Hanford, Wash., August 16–19, 2004.
4. G. Losurdo, "An outlook for Virgo upgrades," presented at the EGO (European Gravitational Observatory) Council, Cascina, Italy, June 16, 2005.
5. S. Saraf, S. Sinha, A. K. Sridharan, and R. L. Byer, "100 W, single frequency, diffraction-limited Nd:YAG MOPA for LIGO," in Conference on Lasers & Electro-Optics (CLEO), Vol. 88 of OSA Trends in Optics and Photonics, A. A. Sawchuk, ed. (Optical Society of America, 2003), pp. 2l45–2147.
6. R. Lawrence, "Active wavefront correction in laser interferometric gravitational wave detectors," Ph. D. dissertation (Massachusetts Institute of Technology, 2003), LIGO-P03000l-00-R.
7. K. Sun and R. L. Byer, "All-reflective Michelson, Sagnac, and Fabry–Perot interferometers based on grating beam splitters," Opt. Lett. **23**, 567–569 (1998).
8. S. Traeger, P. Beyersdorf, L. Goddard, E. Gustafson, M. M.

Fejer, and R. L. Byer, "Polarization Sagnac interferometer with a reflective grating beam splitter," Opt. Lett. **25**, 722–724 (2000).
9. S. Traeger, P. Beyersdorf, E. Gustafson, R. Beausoleil, R. K. Route, R. L. Byer, and M. M. Fejer, "All-reflective interferometry for gravitational-wave detection gravitational waves," AIP Conf. Proc. **523**, 385–386 (2000).
10. P. Beyersdorf, "A polarization Sagnac interferometer for gravitational wave detection," Ph.D. dissertation (Stanford University, 2001).
11. A. Bunkowski, O. Burmeister, P. Beyersdorf, K. Danzmann, R. Schnabel, T. Clausnitzer, E. B. Kley, and A. Tunnermann, "Low-loss grating for coupling to a high-finesse cavity," Opt. Lett. **29**, 2342–2344 (2004).
12. T. Clausnizter, E. B. Kley, A. Tunnermann, A. Bunkowski, O. Burmeister, K. Danzmann, R. Schnabel, A. Duparre, and S. Gliech, "Low-loss gratings for next-generation gravitational wave detectors,"in *Advances in Thin-Film Coatings for Optical Applications II*, M. L. Fulton and J. P. Jruschwitz, eds., Proc. SPIE **5870**, 1–8 (2005).
13. W. Winkler, K. Danzmann, A. Rudiger, and R. Schilling, "Heating by optical absorption and the performance of interferometric gravitational-wave detectors," Phys. Rev. A **44**, 7022–7036 (1991).
14. W. Winkler, "The optics of an interferometric gravitational-wave antenna," in *Proceedings of the 81 WE-Heraeus-Seminar Held at the Physikzentrum Bad Honnef*, J. Ehlers, and G. Schafer, eds. (Springer-Verlag, 1991).
15. P. Hello and J. Y. Vinet, "Analytical models of transient thermoelastic deformations of mirrors heated by high power cw laser beams," French J. Phys. **51**, 2243–2261 (1990).
16. P. Hello and J. Y. Vinet, "Analytical models of thermal aberrations in massive mirrors heated by high power laser beams," French J. Phys. **51**, 1267–1282 (1990).
17. B. W. Shore, M. D. Perry, J. A. Britten, R. D. Boyd, M. D. Feit, H. T. Nguyen, R. Chow, G. E. Loomis, and L. Li, "Design of high-efficiency dielectric reflection gratings," J. Opt. Soc. Am. B **14**, 1124–1136 (1997).
18. R. Tyson, *Principles of Adaptive Optics*, 2nd ed. (Academic, 1998).
19. J. Mansell, J. Hennawi, E. K. Gustafson, M. M. Fejer, R. L. Byer, D. Clubley, S. Yoshida, and D. H. Reitze, "Evaluating the effects of transmissive optic thermal lensing on laser beam quality with a Shack–Hartmann wave-front sensor," Appl. Opt. **40**, 366–374 (2001).
20. M. Abramowitz and I. Stegun, *Handbook of Mathematical Functions* (Dover, 1965).